PHYSICAL REVIEW B **79**, 134302 (2009)

Single-crystal lattice dynamics derived from polycrystalline inelastic x-ray scattering spectra

I. Fischer, A. Bosak, and M. Krisch
European Synchrotron Radiation Facility, B.P. 220, F-38043 Grenoble Cedex, France

(Received 23 September 2008; revised manuscript received 6 February 2009; published 10 April 2009)

We present a methodology to extract the single-crystal phonon dispersion from polycrystalline materials. The approach consists of recording inelastic x-ray scattering (IXS) spectra over a large momentum transfer region (typically $2-80\ \text{nm}^{-1}$), and confront them with a model calculation which properly takes into account the polycrystalline state of the material and the IXS cross section. A least-squares refinement of the model spectra then provides the single-crystal dispersion scheme. For the benchmark cases beryllium and graphite we demonstrate that very good agreement with available single-crystal phonon dispersions is obtained. Furthermore, we show for the case of graphite that a simple texture can be properly taken into account. The proposed method promises to be a valuable tool in cases where single-crystalline materials are not available.

DOI: 10.1103/PhysRevB.79.134302 PACS number(s): 63.20.dd, 63.20.dh, 78.70.Ck

I. INTRODUCTION

Many thermodynamical and elastic properties of a crystal can be understood by investigating the energy of phonons as a function of their momentum transfer throughout the Brillouin zone (BZ). These include equilibrium properties such as thermal expansion, heat capacity and melting, but also transport properties, electron-phonon coupling, as well as elasticity and interatomic forces. The experimental investigation of the phonon dispersion relation, correlating momentum transfer $\vec{Q}$, and energy E of lattice vibrations is the domain of neutron and x-ray spectroscopy. For both techniques, an appropriate selection of the scattering geometry allows the determination of the complete phonon dispersion scheme in single-crystalline materials. In polycrystalline materials, however, the directional information of the momentum transfer $\vec{Q}$ is lost due to the random orientation of the individual crystalline grains. The scattering intensity is integrated over the surface of a shell with a radius equal to the magnitude of $\vec{Q}$, and therefore only averaged properties can be extracted. On one hand the vibrational density of states (VDOS) can be obtained by coherent inelastic neutron scattering (INS)[1] or inelastic x-ray scattering (IXS)[2] in the so-called "incoherent approximation" or by incoherent INS. On the other hand the average longitudinal sound velocity can be investigated if the probing momentum transfer range is chosen to be inside the first BZ.[3] Compared to single-crystal work, the information content is therefore limited. This is an important constraint since novel materials, or materials studied under extreme conditions, are often only available in polycrystalline form because of synthesis procedures or the presence of structural phase transitions. This has motivated researchers to explore methods to obtain detailed information on the lattice dynamics in polycrystalline materials. Two different approaches have been undertaken, both using neutron powder diffraction. The method proposed by Dimitrov *et al.*[4] analyzes the pair distribution function (PDF) obtained by a Fourier transformation of the elastic scattering intensity $S(Q)$. The parameters of a standard phonon model are then refined with respect to the experimental PDF, and the phonon dispersion can be obtained with an accuracy of a few percent. This procedure can, however, only be applied to simple systems[5–7] and requires an appropriate model of the studied system. More recently, Goodwin *et al.*[8] proposed another method. They analyzed reverse Monte Carlo configurations refined to neutron powder-diffraction data. While the extracted phonon dispersion reproduces very well the low-frequency modes, the high-frequency modes cannot be determined precisely. This is due to the fact that optical branches have a small vibrational amplitude and therefore give a small contribution to the diffuse scattering.

The intention of the present work is to overcome these limitations and to develop a methodology to extract the single-crystal phonon dispersion from polycrystalline materials. As a benchmark we have chosen beryllium and textured graphite since they have a favorable IXS cross section and single-crystal phonon dispersions are available. The paper is structured as follows. Section II presents the main theoretical concepts, including the sampling procedure and details of the least-squares refinement. Section III describes the experimental setup and presents the experimental results. Section IV provides the summary and the conclusions.

II. THEORETICAL BACKGROUND

In polycrystalline materials the scattering process takes place on a spherical shell with radius Q in reciprocal space, and the scattering intensity is integrated over the surface of this shell. If the Debye-Waller factors are assumed to be the same for all types of atoms ($\widetilde{W}$) we obtain for the average intensity,[3]

$$S(Q,E,T) = g(Q,E)F(E)\cdot\exp(-2\widetilde{W}), \tag{1}$$

with

$$g(Q,E) = \left\langle \left| \sum_n f_n(Q)M_n^{-1/2}[\vec{Q}\cdot\hat{\sigma}_n(\vec{q},j)] \right|^2 \delta(E \mp E_{\vec{q},j}) \right\rangle, \tag{2}$$

where $f_n(Q)$ is the atomic form factor of atom, n, M_n is the mass, and $\hat{\sigma}_n(\vec{q},j)$ is the normalized phonon eigenvector of mode j with phonon wave vector $\vec{q}$. The upper (lower) sign in the δ function corresponds to the creation (annihilation) of

©2009 The American Physical Society

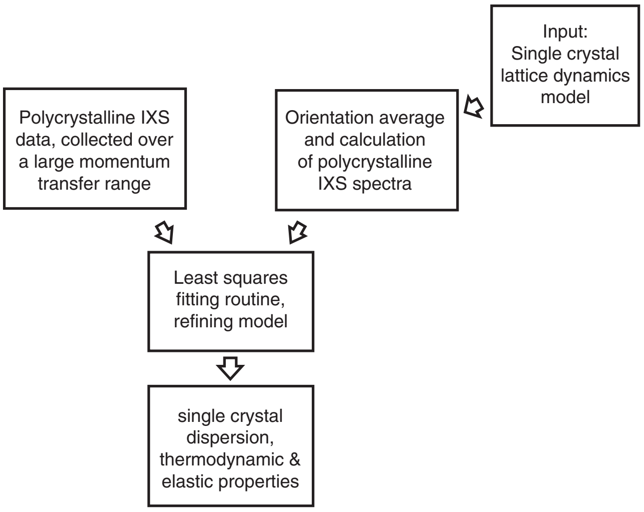

FIG. 1. Schematic concept for the extraction of the single-crystal phonon dispersion from polycrystalline IXS spectra.

a phonon. $\langle \ldots \rangle$ means averaging over the sphere of radius Q and the phonon modes j. The thermal factor is given by

$$F(E) = [\exp(E/k_B T) - 1]^{-1} E^{-1}, \tag{3}$$

where k_B is the Boltzmann constant.

Within the first BZ, the reciprocal lattice vector τ is equal to zero, which leads to $\vec{Q} = \vec{q}$ and the scalar product in Eq. (2) becomes

$$|\vec{q} \cdot \hat{\sigma}_n(\vec{q}, j)|^2. \tag{4}$$

This imposes the constraint that only components of the eigenvector parallel to the phonon propagation contribute to the dynamical structure factor. For pure longitudinal acoustic (LA) phonons, propagation and eigenvector are parallel to each other, and they dominate the inelastic scattering spectrum, whereas pure transverse acoustic (TA) phonons do not contribute. For large momentum transfers $g(Q,E)$ approaches the phonon density-of-states limit,

$$g(Q,E) \to AQ^2 \cdot \sum_n \frac{G_n(E)}{M_n} \cdot f_n^2(Q), \tag{5}$$

where $G_n(E) = \Sigma_{\vec{q},j} |\hat{\sigma}_n(\vec{q}, j)|^2 \delta(E - E_{\vec{q},j})$ are the partial density of states and A is a scaling factor.[2] In between the low Q and the density-of-states limit, the IXS spectra still display a marked Q dependence due to—though relaxed—selection rules. It can therefore be expected that the information contained in the IXS spectra spanning a large Q range allows a critical test of a lattice dynamics model. This forms the basis of our proposed methodology.

The main concept of the method is illustrated in Fig. 1. On one side IXS data from the polycrystalline material are recorded over a large momentum transfer range. On the other side a theoretical model of the lattice dynamics in the single crystal is required. Here, we utilized a Born–von Kármán model,[9] whose force constants, describing the interactions between neighboring atoms, are refined via a least-squares fitting routine to the experimental polycrystalline IXS spectra. The refined set of force constants can then be utilized to calculate the single-crystal phonon dispersion and to extract elastic and thermodynamic properties. The starting parameters for the fitting routine are crucial for the success of the method. In order to prove the validity of the method and explore its limitations, a set of force constants derived from existing single-crystal dispersions was taken.

The intensity scattered from a polycrystalline sample, which is composed of randomly orientated crystallites, is the sum of the contributions from these crystallites. The directional information of the momentum transfer $\vec{Q}$ is therefore lost, and the inelastic scattering intensity has to be computed by integrating over the surface of a sphere with radius $|\vec{Q}| = Q_{\text{mag}}$. The integration is performed, summing up discrete contributions on the irreducible section of the sphere. The size of the section is given by the symmetry of the material. A proper sampling over this surface with a uniform mesh of points without gap or overlap is necessary. We have chosen a mesh with a constant step size ($\Delta\varphi = \Delta\theta = \text{const.}$) in the Euler angles φ and θ and $N_{\Delta\varphi}$ and $N_{\Delta\theta}$ nodes, respectively. The sampled $\vec{Q}$ points are situated in the center of the thus created sections of the sphere. It can be shown that the area of a single section $S_{\text{point}}(\theta)$ is given by

$$S_{\text{point}}(\theta) = 2\pi Q_{\text{mag}}^2 [\cos(\theta) - \cos(\theta - \Delta\theta)]/N_{\Delta\rho}, \tag{6}$$

$$= 2\pi Q_{\text{mag}}^2 \Delta\theta \sin(\theta)/N_{\Delta\varphi}. \tag{7}$$

This implies that each node has to be weighted by $\sin(\theta)$. Moreover, attention was paid that none of the $\vec{Q}$ points coincides with high-symmetry directions in order to avoid singularities in the computed intensity distribution.[10] The dynamical matrix was diagonalized for each $\vec{Q}$ point, and the obtained frequencies and eigenvectors were used to compute the scattered intensity. Finally, the IXS intensities of all sampled $\vec{Q}$ points were summed up, considering the weighting factor $\sin(\theta)$, and the obtained intensity distribution was convoluted with the experimental resolution function.

The model calculations were refined to the experimental IXS spectra via a least-squares fitting routine. The fitting parameters were the force constants a_N, the elements of the dynamical matrix. The maximum likelihood estimate of the model parameters is obtained by minimizing the merit function χ^2,

$$\chi^2 = \sum_{i=1}^{N} \left(\frac{y_{\text{exp}}(x_i) - y_{\text{mod}}(a_N, x_i)}{\sigma_i} \right)^2, \tag{8}$$

where y_{exp} is the experimental intensity and y_{mod} is the modeled intensity for the energy transfer x_i. We used the Levenberg-Marquardt algorithm,[11,12] which is an effective way to solve nonlinear least-squares problems,[13] and is relatively rapidly converging. Depending on the number of force constants (graphite: 17; beryllium: 29), one fitting session took between 60 and 90 h on a HP Proliant dual core computer (2.6 GHz, 8 GB RAM). In order to optimize the computing time, the program was parallelized whereby the computing time could be reduced by a factor corresponding to the number of force constants.

Our modeling is performed within the frame of one-phonon scattering. For IXS this assumption is largely valid. In fact, the ratio of two-phonon to one-phonon scattering is equal to $1/2Q_iU^{ij}Q_j$, where U^{ij} is the thermal displacement parameter and Q_i is the momentum transfer. Taking available literature values for U_{ij} we obtain an integral contribution of two-phonon scattering amounting to 9% for graphite and beryllium at $Q=50\ \text{nm}^{-1}$. This adds a smooth, weakly modulated background and does not alter the spectral shape. The direct calculation of multiphonon contributions is computationally very expensive and was not considered in the present study for the reasons outlined above.

III. EXPERIMENTAL RESULTS

A. Polycrystalline beryllium

The IXS experiment was performed on beamline ID28 at the European Synchrotron Radiation Facility, utilizing the silicon (999) backscattering configuration with an energy resolution of 3.0 meV. The x rays were focused by a toroidal mirror to a spot size of $250\times 60\ \mu\text{m}^2$ (horizontal *x* vertical, full width at half maximum). A total of 90 IXS spectra was recorded, spanning a momentum transfer region from 1.9 to 79.5 nm^{-1}. Counting times varied between 20 and 60 s/point, resulting in typical IXS scan lengths of 1–3 h. We chose the exact angular positions to uniformly cover the achievable momentum transfer range and to avoid Bragg peaks. The resolution functions were experimentally determined from a poly(methylmethacrylate) (PMMA) sample kept at 10 K and at $Q=10\ \text{nm}^{-1}$. Furthermore, relative efficiencies of the analyzers were determined using the elastic scattering from a PMMA sample at the same angular position of the spectrometer as the ones used for the ensemble of IXS spectra. The sample was a compressed pellet of beryllium grains of 15 mm diameter (and 3 mm height), corresponding roughly to one absorption length, $t_\mu=1/\mu$, where μ is the photoelectric absorption coefficient. Due to the large grain size it was necessary to rotate the sample around an axis, parallel to the disk axis, with a frequency of about 10 Hz in order to obtain a good powder average. The absence of texture was verified determining the relative intensities of the Debye-Scherrer rings and comparing them to the ideal powder x-ray diffraction spectrum.

The complete experimental momentum transfer-energy-intensity map is shown in Fig. 2. The experimental data are normalized to the incoming x-ray intensity, the polarization of the beam, the analyzer efficiencies, and the atomic form factor. Furthermore, the elastic line was carefully subtracted using a pseudo-Voigt fit. In the low Q limit the dispersion of the averaged longitudinal dynamics is observable, while in the high Q limit the VDOS is approached. In the intermediate momentum transfer range and lower energy region acoustic phonons form the arc structure. Optical vibrations compose the band in the higher energy range. The Q values of the IXS spectra, selected for the refinement procedure, are marked by a white line (Q=3.2, 8.0, 14.4, 19.3, 22.9, 42.8, 52.2,62.6, 69.4, and 78.5 nm^{-1}). A Born–von Kármán lattice dynamics model was refined to the ten spectra, using the beryllium hexagonal unit cell with $a=2.2858$ Å and $c=3.5843$ Å, and two atoms at (0,0,0) and (1/3,2/3,0.5). We have included up to the seventh nearest-neighbors (NN) atomic force constants (29 parameters), using as starting parameter the set of force constants published in Ref. 14. These were obtained from a least-squares fit of a Born-von Kármán model to the experimental INS dispersion.[15] The scattering intensity was calculated for a mesh of 43 200 points on 1/24 of the spherical shell surface and then averaged and properly weighted as described above. The merit function decreased by a factor of 2.4 from $\chi^2_{\text{start}}=3.73$ to $\chi^2_{\text{end}}=1.55$. In Fig. 3 six representative experimental IXS spectra are displayed together with the resulting computed spectra using the starting and refined model. It can be noted that already the starting model shows a remarkable agreement with the experimental data; improvements in the refined model are nevertheless evident. At low momentum transfers (3.2, 8.0 nm^{-1}) the positions of the peaks are improved. For the spectrum at 14.4 nm^{-1} the intensity distribution of the main feature at about 77 meV is better reproduced. Finally, a better agreement can be appreciated for the low-energy portion in the spectrum at 62.6 nm^{-1}.

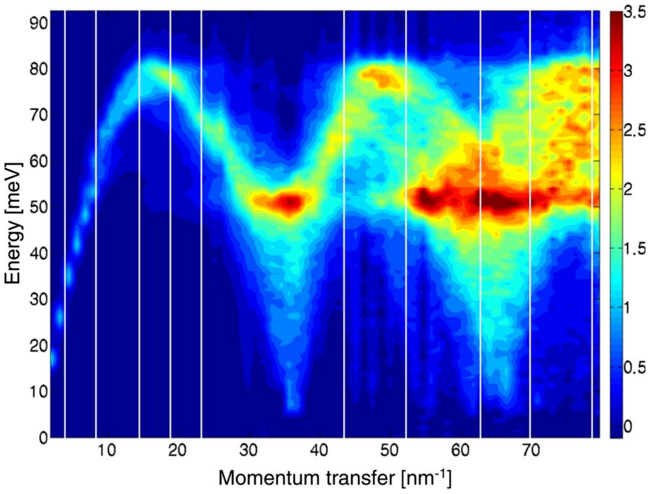

FIG. 2. (Color online) Experimental IXS intensity map of beryllium, composed of constant momentum transfer scans. The spectra are normalized, and the elastic line is subtracted. The white lines indicate the ten selected spectra used for the fitting routine.

Figure 4 confronts the dispersion calculated from the refined force constants (red line) with the experimental one (black dots) and the starting model (blue line). The excellent overall agreement confirms the results obtained for the polycrystalline system. Differences can be observed in the optical branches. This is due to the fact that the shape of the optic part in the IXS spectra is more sensitive to the choice of the number of neighbors and the set of force constants, illustrating the limitation of the Born–von Kármán model in this very anisotropic system.

It is important to note that even without a refinement as described above, a stringent discriminating test can be made if several lattice dynamics models exist. This is actually the case for beryllium, for which, besides the force constants of Hannon *et al.*,[14] another set has been derived by Kwasniok.[16] Kwasniok[16] utilized 33 parameters including up to the eighth nearest neighbors, while Hannon *et al.*[14] refined 29 param-

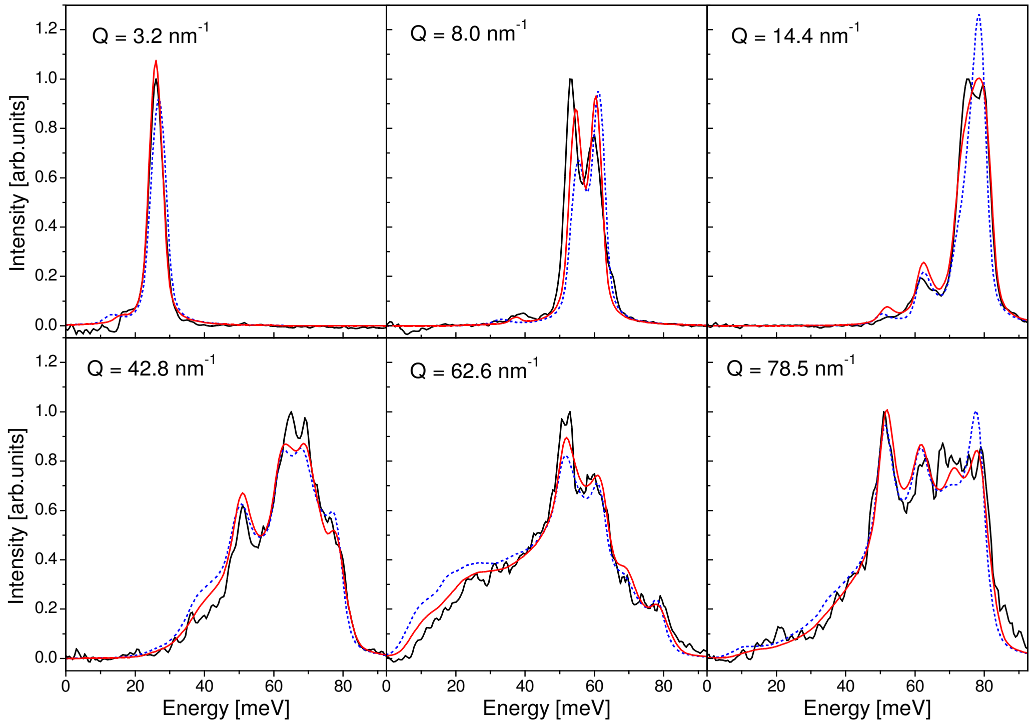

FIG. 3. (Color online) Polycrystalline IXS spectra: experiment (black line), starting model spectra (blue line, dashed), and refined model spectra (red line, gray).

eters considering 7 next neighbors. The two calculations show an equally good agreement with the experimental data for the main symmetry directions of the phonon dispersion. In contrast to this, the computed individual IXS spectra show distinct differences as can be appreciated in Fig. 5, which shows four representative spectra. Obvious discrepancies in peak positions and intensities occur for the model of Kwasniok[16] in all spectra. On the contrary, the calculation of Hannon *et al.*[14] reproduces the spectra quite well throughout the whole Q region. This observation can be understood considering that in the INS dispersion only main symmetry directions are taken into account, whereas the calculation of the polycrystalline IXS spectra involves also nonhigh-symmetry directions. The additional information from these directions allows making the appropriate choice between different models.

The model calculations furthermore allow the determination of the elasticity tensor. In fact, the five independent elastic moduli C_{11}, C_{33}, C_{44}, C_{66}, and C_{13} can be derived from the initial slope of the acoustic phonon branches, using the Christoffel equation.[17] The thus obtained values are reported in Table I, together with previous experimental[19–21] and theoretical results.[18] A formally correct evaluation of the error bars was not possible due to the large number of fitting parameters, their correlation, and the lack of a simple relationship between the refined force constants and the elastic moduli. We therefore provide only a qualitative discussion. The best agreement is obtained with the experimental results of Rowlands and White[20] (about 7%–9% for C_{11} and C_{33}, and 16% and 20% for C_{44} and C_{66}, respectively). The value for C_{13}, however, displays a large discrepancy, compared to all other results. This can be understood since the extraction of C_{13} from measured sound velocities requires the knowledge of the other four independent elastic moduli and explains as well the large scatter of the other experimental results. In order to probe the influence of constraining parameters, we introduced the bulk modulus K and C_{44} as additional experimental values. The choice of these two parameters was motivated by the fact that they can be obtained from polycrystalline data via x-ray diffraction and Raman scattering, respectively. In fact, phenomenological modeling shows that the Raman-active mode can be approximately correlated with the transverse acoustic phonon, directly linked to C_{44}.[22] Both parameters were weighted in such a way that each has the same importance as one of the ten IXS

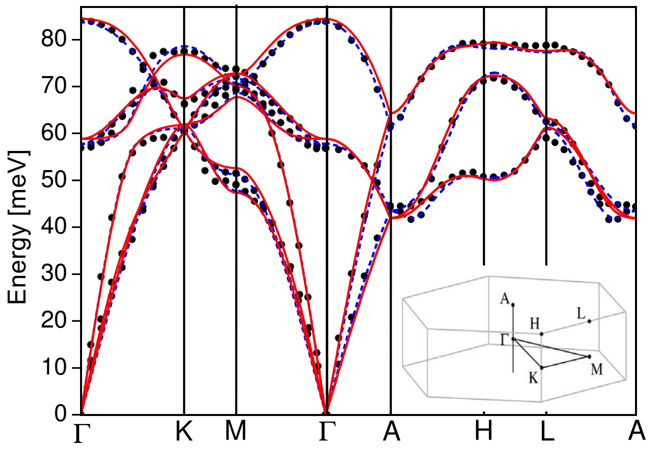

FIG. 4. (Color online) Dispersion relation for beryllium: experimental INS data (black dots) (Ref. 15), starting model (blue line, dashed), and refined model calculation (red line, gray).

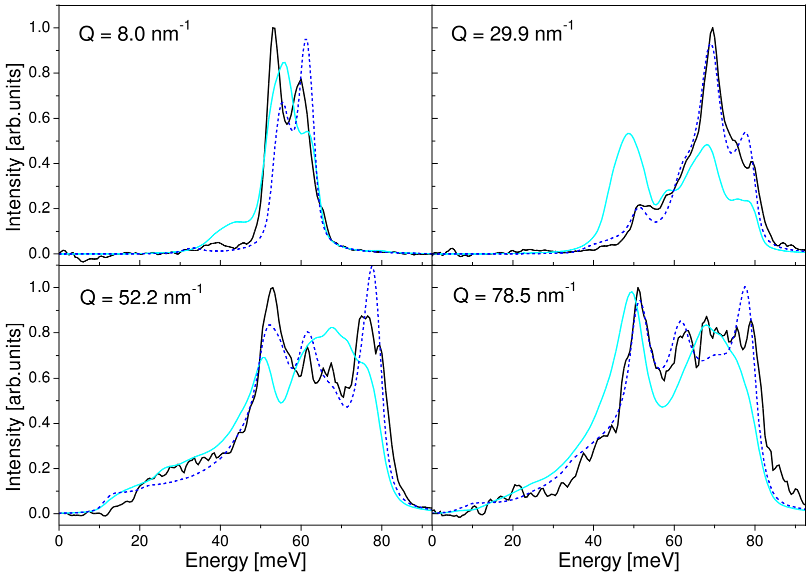

FIG. 5. (Color online) IXS spectra from polycrystalline beryllium (black line) compared to model calculations using force constants published by Hannon *et al.* (Ref. 14) (blue line, dashed) and by Kwasniok (Ref. 16) (light blue line, gray).

spectra. We used $K=116.8$ GPa and $C_{44}=162.2$ GPa (Ref. 19) for the fitting procedure. The thus obtained moduli are reported as well in Table I. We note a drastic improvement for C_{13}, whereas the other moduli show only moderate variations between 3 and 12%. In fact, again the best agreement is obtained for the data set of Rowlands and White.[20] In general, the obtained elastic moduli are in good agreement with single-crystal experiments, keeping in mind that these single-crystal properties are extracted from experimental data from a polycrystalline material.

B. Textured graphite

A further important test for the validity of the proposed methodology is the inclusion of a simple texture. Pyrolytic graphite was chosen since it is a simple, strongly textured system, and significant deviations of the inelastic scattering intensity from the homogenous polycrystalline system can be expected. The pyrolytic graphite sample of 8 mm diameter (corresponding roughly to one absorption length) was rotated with a frequency of about 10 Hz around an axis, perpendicular to the crystallographic c axis and the horizontal scattering plane. In this way, all crystallographic directions are probed, and only a simple texture needs to be introduced (see below). The same instrumental setup as in the case for beryllium was utilized. Altogether 70 experimental IXS spectra were recorded for the energy loss side including the elastic line, centered at zero energy transfer, in the momentum transfer range from 1.9 to 77.0 nm^{-1}. Data acquisition times were comparable to the ones for beryllium.

In order to visualize features at higher energy transfer E the intensity of the experimental intensity map (Fig. 6) was scaled: $I_{\mathrm{Map}}=I_{\mathrm{Exp}}\cdot E$. Furthermore, the same raw data corrections as in the case of Be were performed. The map shows a pronounced arc structure in the low-energy part (up to 20 meV), mainly formed by the phonon dispersion along the $\Gamma-A$ direction. The dominance of these phonons is due to the strong texture, induced by the rotation of the sample in the experiment. In contrast to beryllium, a part of the optic branches (mainly along $\Gamma-A$) is superposed to acoustic vibrations in arbitrary directions, both occupying the same energy transfer range. Above about 20 meV only in-plane vibrations contribute to the intensity. The white lines in Fig. 6 indicate the ten spectra used in the refinement procedure ($Q=3.2$, 8.0, 12.8, 16.3, 28.0, 38.9, 41.3, 47.1, 57.8, and 69.3 nm^{-1}).

TABLE I. Elastic constants of Beryllium in GPa. Error bars are indicated whenever available.

	C_{11}	C_{33}	C_{44}	C_{66}	C_{13}
Refined dispersion	268.8	321.5	122.3	96.7	96.7
Refined dispersion (with K and C_{44})	255.9	343.5	156.1	93.7	3.57
Model dispersion (Ref. 14)	273.1	282.5	144.5	86.2	141.3
Robert and Sollier (Ref. 18), theory	305.9	329	159.3	143.6	10.4
Migliori *et al.* (Ref. 19), experiment	293.6(18)	356.7(21)	162.2 (3)	133.4(16)	14.0 (11)
Rowlands and White (Ref. 20), experiment	288.8(25)	354.2(25)	154.9(25)	134.4(30)	4.7 (5)
Smith and Arbogast (Ref. 21), experiment	292.3	336.4	162.5	132.8	14.0

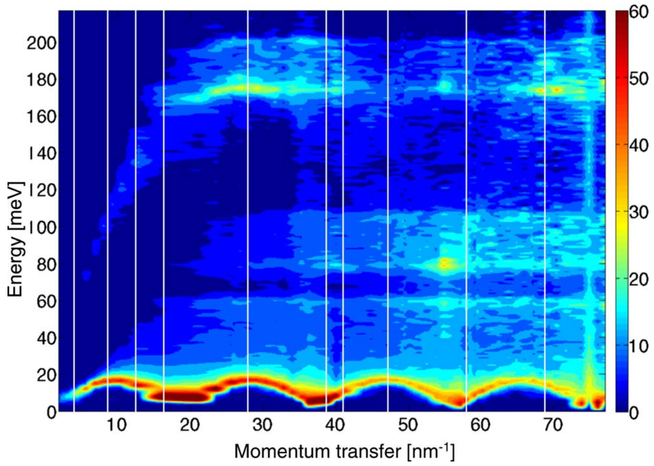

FIG. 6. (Color online) Experimental IXS intensity map of pyrolythic graphite. The spectra are normalized, and the elastic line is subtracted. The white lines mark the ten selected spectra used for the fitting routine.

Graphite has a hexagonal unit cell with atoms at position [0,0,0], [2/3,1/3,0], [0,0,1/2], and [1/3,2/3,1/2], and basis vectors $a=2.462$ Å and $c=6.711$ Å. We used a Born–von Kármán model with 17 force constants, including up to the sixth nearest neighbor, taking literature values as starting parameters.[23–25] For the simple texture of the sample, the orientation matrix g is given by[26]

$$g=\begin{pmatrix}1 & 0 & 0\\ 0 & \cos(\theta) & \sin(\theta)\\ 0 & -\sin(\theta) & \cos(\theta)\end{pmatrix}\begin{pmatrix}\cos(\varphi) & \sin(\varphi) & 0\\ -\sin(\varphi) & \cos(\varphi) & 0\\ 0 & 0 & 1\end{pmatrix}, \qquad (9)$$

where the angles θ, φ, and ψ correspond to the Euler angles. The orientation distribution in a polycrystalline material is mathematically represented by the orientation distribution function $f(g)$, which is in our case,

$$f(g)=\frac{4}{\sin(\theta)}\delta(\psi). \qquad (10)$$

The orientation distribution function is normalized,

$$\int f(g)dg=1, \qquad (11)$$

with

$$dg=d\rho d\theta d\psi\,\sin(\theta)/8\pi^2 \quad (0\le\varphi;\psi\le 2\pi;0\le\theta\le\pi). \qquad (12)$$

Such a configuration is equivalent to the study of a textured sample with a weighting function $W(\theta)=1/\sin(\theta)$, where θ is the angle between the incident beam and the c axis. Considering the experimental geometry one obtains for the scattered intensity,

$$\langle I(E)\rangle=\int I(\theta,\varphi,E)f(g)dg. \qquad (13)$$

This texture is easy to implement in the modeling. In Fig. 7 the experimental spectra (black line) are compared to two model calculations: one computed with a uniform distribution of crystallographic directions (yellow line) and the other one including texture (blue line). Clear changes in the relative intensities between the model with and without texture can be observed. The peak at low-energy transfer, due to vibrations along the $\Gamma-A$ direction, becomes more pronounced, while the inelastic features at higher energy transfer, mainly due to vibrations within the basal plane, are weakened in the case of the textured system. Generally, the intensity due to vibrations along $\Gamma-A$ is amplified as a result of the texture, whereas the peak positions are independent of

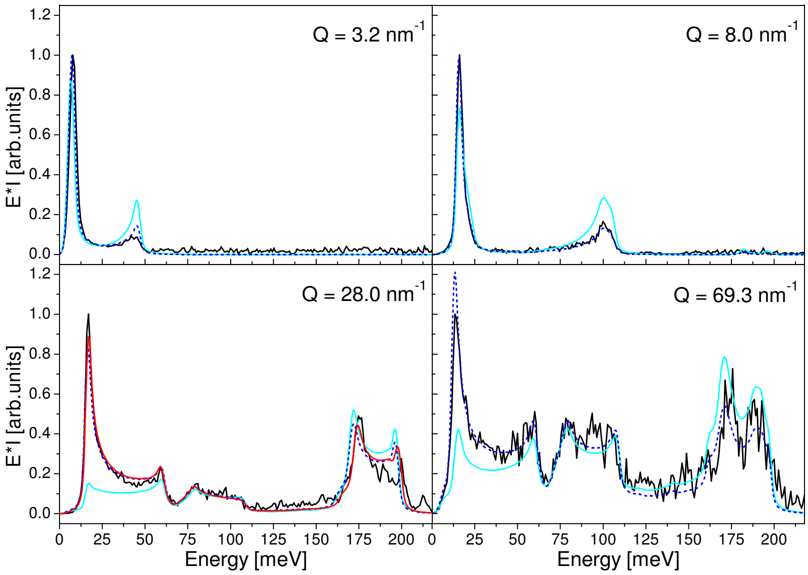

FIG. 7. (Color online) Comparison of the graphite experimental data (black line) with the model without considering texture (light blue line, light gray) and including texture (blue line, dashed). For $Q=28.0$ nm^{-1} the spectrum for the refined model is as well shown (red line, gray). (i) The IXS intensity was multiplied by (e) the energy for better visualization of the optical modes.

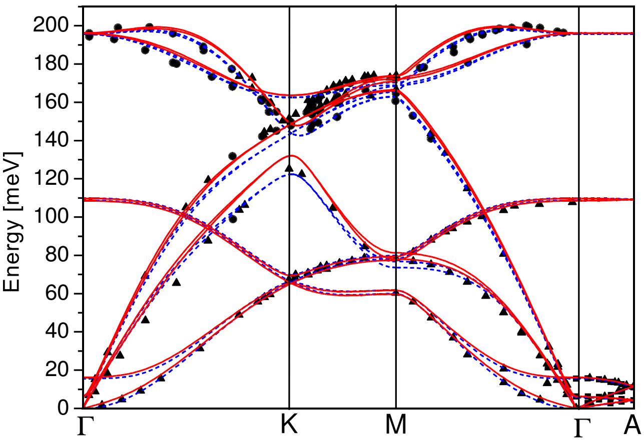

FIG. 8. (Color online) Dispersion relation of graphite along the main symmetry directions: INS (pyrolytic graphite) (black squares) (Ref. 23), single-crystal IXS [black triangles (Ref.) and circles (Ref. 27)], starting model (blue line, dashed) and refined model (red line, gray).

the texture. The comparison of the two calculated inelastic spectra underlines the importance to consider texture in the model calculation. During the refinement procedure we noted that the energy of the highest optical branch showed significant deviations with respect to the single-crystal dispersion. We therefore included the energy of the highest optical branch at the Γ point ($E=196.1$ meV) as further experimental constraint (with the weight of one experimental spectra). This improved the agreement of the highest energy optical phonon branches, mainly around the Γ point. The merit function decreased by a factor of 1.7 from $\chi^2_{\text{start}}=3.34$ to $\chi^2_{\text{end}}=1.95$.

Figure 8 shows the model and the refined phonon dispersion in comparison with previous single-crystal results.[23,24,27] The most obvious difference between the refined dispersion and the experimental one is along the $\Gamma-K$ direction. Here, the energy of longitudinal acoustic and transverse acoustic branches is too high on approaching the K point (at about 130 meV, while the single-crystal experiment yields 125 meV). Nevertheless, the refined model improved the agreement for the transverse optic branch, just above, compared to the model published by Mohr *et al.*[24] Furthermore, the refined dispersion in the higher optical part (above 140 meV) changed with respect to the starting model for the $K-M$ direction, but since the trend of the experimental data is ambiguous in this region, one cannot conclude on an improvement.

As for beryllium we derived the elastic moduli from the initial slope of the acoustic branches. The obtained values are presented in Table II. C_{11} is significantly lower (19%) than the one obtained by INS.[23] One should be aware that the INS experiment was performed on a pyrolytic graphite sample. Thus, the in-plane LA branch is the least reliable in this experiment due to the nature of the sample. On the other hand, the obtained C_{11} is in good agreement with IXS results from a single-crystal flake.[28] We note an equally good agreement for C_{33} and C_{44}. C_{66} is significantly higher than the values obtained from a single (pyrolytic) crystal by IXS (Ref. 28) and INS,[23] respectively. This is a consequence of the steeper dispersion of the in-plane polarized TA branch along $\Gamma-K$ from which C_{66} was extracted. Consequently, the value derived in the frame of the present work is too high. As for beryllium C_{13} is poorly defined, and we therefore did not attempt to determine it.

IV. CONCLUSIONS AND OUTLOOK

We have presented a methodology for the determination of the complete lattice dynamics from polycrystalline materials, using inelastic x-ray scattering. It could be shown that for the chosen simple test cases beryllium and graphite a least-squares refinement of a model calculation can be performed. The refined phonon dispersion curves are in very good agreement with existing results, obtained by "conventional" single-crystal inelastic neutron and/or x-ray scattering. A reasonably good starting model is essential for the fit to converge. In general there are several possibilities to produce suitable starting parameters. One is to use force constants of the material, if they are available, or, alternatively, of a system with similar physical properties. Another option is to use empirical models such as rigid-ion or shell models. Finally, a set of Hellmann-Feynman forces can be computed, using *ab initio* methods. It is important to stress that the proposed methodology is limited to relatively simple materials. As the number of atoms per unit cell increases, the density of phonon branches increases, and distinct features can no longer be observed in the polycrystalline IXS spectra, making a refinement fit impossible. A further constraint arises if the material is composed of light and heavy atoms. As the IXS cross section is roughly proportional to Z^2, where Z is the number of electrons, the weak signal from the light atom species is masked by the strong signal arising from the heavy atom species.

It has been demonstrated that even without a fit procedure the validity of a model calculation can be assessed by inspection of individual polycrystalline inelastic spectra. As a matter of fact, a comparison (experiment versus model/theory) of not only the phonon energies but also the intensity distri-

TABLE II. Comparison of the elastic constants for graphite from polycrystalline IXS data with previous experimental and theoretical values. All values are in GPa. Error bars are indicated whenever available.

	C_{11}	C_{12}	C_{13}	C_{33}	C_{44}	C_{66}
Present work	1161	17.8		39.7	5.58	571.6
Bosak *et al.* (Ref. 28)	1109 (16)	139 (36)	0 (3)	38.7(7)	5.0 (3)	485 (10)
Nicklow *et al.* (Ref. 23)	1440 (220)			37.1(5)	4.6 (2)	460
Boettger (Ref. 29)	$C_{11}+C_{12}=1280$		−0.5	40.8	4.5	

bution, and furthermore including all crystallographic directions (as we deal with a polycrystalline material), provides an important constraint.

We have furthermore shown for the case of graphite that texture can be included in the refinement procedure. This aspect is of relevance since polycrystalline materials are quite commonly textured. As long as the texture is homogeneous within the probed sample volume, and it is well characterized, the inclusion of the texture does not add any more complexity in the refinement procedure from a computational point of view.

Another important point concerns the determination of the single-crystal elastic tensor. In general we note that the agreement for the longitudinal moduli, here C_{11} and C_{33}, is very good: within 10% for Be and 4% for graphite. On the other hand, the other moduli display significantly larger deviations. This is due to the fact that the transverse acoustic dynamics are reflected in the IXS spectra as low-energy cutoffs and not as well defined peaks as is the case for the longitudinal acoustic dynamics. The agreement can be improved by the inclusion of further experimental available quantities in the fitting routine. Here, we utilized the bulk modulus and the Γ-point phonon energies, which can be obtained by x-ray diffraction and Raman spectroscopy, respectively. Nevertheless, taking into account that the elastic moduli are derived from a (textured) polycrystalline material, the result is more than satisfactory.

The proposed methodology, aiming at the extraction of the complete lattice dynamics from polycrystalline materials, promises to find applications in several research fields. In particular the study of materials in extreme conditions of temperature and/or pressure is often only possible in the polycrystalline state. The method will considerably benefit from the next generation of IXS spectrometers. In particular a multianalyzer crystal spectrometer, covering the entire momentum transfer range, would allow the collection of all the IXS spectra simultaneously, consequently significantly reducing the data acquisition time. Finally, it is important to note that the method can be equally well applied to coherent inelastic neutron scattering with the exception of the low-momentum-high-energy transfer range which is difficult to access with neutrons due to kinematic limitations and experiments at very high pressures (beyond 10 GPa) for which the required small sample volume is not sufficient for INS studies. Joint IXS-INS studies appear in particular promising for materials containing elements with strongly different scattering strengths for x rays and neutrons, and systems where the magnetic and lattice excitations need to be disentangled.

---

[1] G. L. Squires, *Introduction to the Theory of Thermal Neutron Scattering* (Cambridge University Press, Cambridge, 1978).

[2] A. Bosak and M. Krisch, Phys. Rev. B **72**, 224305 (2005).

[3] A. Bosak, M. Krisch, I. Fischer, S. Huotari, and G. Monaco, Phys. Rev. B **75**, 064106 (2007).

[4] D. A. Dimitrov, D. Louca, and H. Roder, Phys. Rev. B **60**, 6204 (1999).

[5] W. Reichardt and L. Pintschovius, Phys. Rev. B **63**, 174302 (2001).

[6] M. J. Graf, I. K. Jeong, D. L. Starr, and R. H. Heffner, Phys. Rev. B **68**, 064305 (2003).

[7] I. K. Jeong, R. H. Heffner, M. J. Graf, and S. J. L. Billinge, Phys. Rev. B **67**, 104301 (2003).

[8] A. L. Goodwin, M. G. Tucker, M. T. Dove, and D. A. Keen, Phys. Rev. Lett. **93**, 075502 (2004).

[9] M. Born and K. Huang, *Dynamical Theory of Crystal Lattices* (Oxford University Press, Oxford, 1954).

[10] L. Van Hove, Phys. Rev. **89**, 1189 (1953).

[11] K. Levenberg, Q. Appl. Math. **2**, 164 (1944).

[12] D. W. Marquardt, J. Soc. Ind. Appl. Math. **11**, 431 (1963).

[13] W. H. Press, S. A. Teukolsky, W. T. Vetterling, and B. P. Flannery, *Numerical Recipes in C: The Art of Scientific Computing* (Cambridge University Press, Cambridge, 1992).

[14] J. B. Hannon, E. J. Mele, and E. W. Plummer, Phys. Rev. B **53**, 2090 (1996).

[15] R. Stedman, Z. Amilius, R. Pauli, and O. Sundin, J. Phys. F: Met. Phys. **6**, 157 (1976).

[16] F. Kwasniok, Surf. Sci. **329**, 90 (1995).

[17] B. A. Auld, *Acoustic Fields and Waves in Solids* (J. Wiley and Sons, New York, 1973), Vol. 1.

[18] G. Robert and A. Sollier, J. Phys. IV **134**, 257 (2006).

[19] A. Migliori, H. Ledbetter, D. J. Thoma, and T. W. Darling, J. Appl. Phys. **95**, 2436 (2004).

[20] W. D. Rowlands and J. S. White, J. Phys. F: Met Phys. **2**, 231 (1972).

[21] J. F. Smith and C. L. Arbogast, J. Appl. Phys. **31**, 99 (1960).

[22] S. Merkel, A. F. Goncharov, H. K. Mao, P. Gillet, and R. J. Hemley, Science **288**, 1626 (2000).

[23] R. Nicklow, H. G. Smith, and N. Wakabaya, Phys. Rev. B **5**, 4951 (1972).

[24] M. Mohr, J. Maultzsch, E. Dobardzic, S. Reich, I. Milosevic, M. Damnjanovic, A. Bosak, M. Krisch, and C. Thomsen, Phys. Rev. B **76**, 035439 (2007).

[25] Mohr *et al.* (Ref. 24) provided a set of force constants up to the fifth next neighbor for the two-dimensional graphene sheet, while Nicklow *et al.* (Ref. 23) determined a set of force constants up to the fourth next neighbor for graphite.

[26] S. Matthies and M. Humbert, J. Appl. Crystallogr. **28**, 254 (1995).

[27] J. Maultzsch, S. Reich, C. Thomsen, H. Requardt, and P. Ordejon, Phys. Rev. Lett. **92**, 075501 (2004).

[28] A. Bosak, M. Krisch, M. Mohr, J. Maultzsch, and C. Thomsen, Phys. Rev. B **75**, 153408 (2007).

[29] J. C. Boettger, Phys. Rev. B **55**, 11202 (1997).